Title: Heparin molecularly imprinted polymer thin flm on gold electrode by plasma-induced graft polymerization for label-free biosensor

Authors: Kouhei Orihara, Atsushi Hikichi, Tomohiko Arita, Hitoshi Muguruma, Yasuo Yoshimi

PII: S0731-7085(17)32549-9
DOI: https://doi.org/10.1016/j.jpba.2018.01.012
Reference: PBA 11726

To appear in: *Journal of Pharmaceutical and Biomedical Analysis*

Received date: 11-10-2017
Revised date: 24-12-2017
Accepted date: 8-1-2018

Please cite this article as: Kouhei Orihara, Atsushi Hikichi, Tomohiko Arita, Hitoshi Muguruma, Yasuo Yoshimi, Heparin molecularly imprinted polymer thin flm on gold electrode by plasma-induced graft polymerization for label-free biosensor, Journal of Pharmaceutical and Biomedical Analysis https://doi.org/10.1016/j.jpba.2018.01.012

Heparin molecularly imprinted polymer thin flm on gold electrode by plasma-induced graft polymerization for label-free biosensor

Kouhei Orihara, Atsushi Hikichi, Tomohiko Arita, Hitoshi Muguruma*, Yasuo Yoshimi

Graduate School of Engineering and Science, Shibaura Institute of Technology, 3-7-5 Toyosu, Koto, Tokyo 135-8548, Japan

*Corresponding Author.

*****E-mail address: muguruma@shibaura-it.ac.jp (H. Muguruma).

Molecularly imprinted polymer

Plasma-induced polymerization

Surface imprinting

Graphical abstract

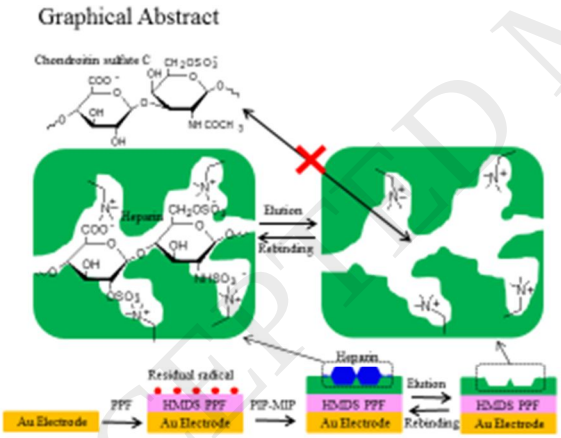

Highlights

- A label-free quartz crystal microbalance biosensor for heparin detection based on a macro-molecularly imprinted polymer (MIP) as an artificial recognition element is addressed.
- The novel strategy for MIP in the form of thin film on a gold electrode with the plasma-induced graft polymerization (PIP) technique is demonstrated.
- The heparin-PIP-MIP as a synthetic antibody specifically binds to heparin and can be applied to biosensor.

ABSTRACT

Heparin, a highly sulfated glycosaminoglycan, is an important biomaterial having biological and therapeutic functionalities such as anticoagulation, regeneration, and protein stabilization. This study addresses a label-free quartz crystal microbalance (QCM) biosensor for heparin detection based on a macro–molecularly imprinted polymer (MIP) as an artificial recognition element. We demonstrate the novel strategy for MIP in the form of thin film on a gold (Au) electrode with the plasma-induced graft polymerization (PIP) technique. The procedure of PIP is as follows: (i) Hexamethyldisiloxane plasma-polymerized thin film (PPF) as a pre-coating scaffold of active species for PIP (post-polymerization) is deposited on an Au electrode. (ii) The PPF/Au electrode is soaked in an water solution containing heparin (template), (2-(methacryloxy)-ethyl)trimethylammonium chloride acrylamide (functional monomer), acrylamide, and N,N-methylenebisacrylamide (crosslinker). Double bonds of monomer and crosslinker attacked by residually active species in pre-coating PPF cause radical chain reaction. Consequently, a growing polymer network of 20 nm thickness of PIP-MIP thin film is formed and grafted on the PPF/Au surface. (iii) The PIP-MIP/PPF/Au is washed by sodium chloride solution so as to remove the template. Non-imprinted polymer (NIP) is carried out like the same procedure without a template. The AFM, XPS, and QCM measurements show that the PIP process facilitates macro–molecularly surface imprinting of template heparin where the template is easily removed and is rapidly rebound to PIP-MIP without a diffusional barrier. The heparin-PIP-MIP specifically binds to heparin compared with heparin analog chondroitin sulfate C (selective factor: 4.0) and a detectable range of heparin in the presence of CS (0.1 wt%) was 0.001-0.1 wt%. The PIP-NIP does not show selectivity between them. The evaluated binding kinetics are association (k_a=350±100 $M^{-1} s^{-1}$), dissociation (k_d=(5.0±2.0) × 10^{-4} s^{-1}), and binding (K_D=1.3±0.6 μM) constants, demonstrating that the PIP-MIP as a synthetic antibody can be applied to analytical chemistry.

Keywords: Heparin

1. Introduction

Molecularly imprinted polymers (MIPs) are obtained by the co-polymerization of functional monomer(s) and a crosslinker in the presence of a target molecule, which is called a template. Subsequently, when the template is removed (washed out), the template ghost cavity can easily interact with the original template where the positions of functional groups and the shape of the template are memorized in the polymer network. To date, MIPs of low-molecular mass template are routine work; in fact, numerous MIPs of low-molecular mass template are applied to sensors/analyses and separations/extractions [1]. However, fabrication of "macro"-molecularly imprinted polymers is still a challenging task [2] for the following reasons: (i) The macromolecularly imprinted polymers (for which the template is often a biomacromolecule) must be done in an aqueous medium, unlike the MIPs of low-molecular mass template, which is often done in a nonpolar solvent, which limits the selection of functional monomer and crosslinker. (ii) The interaction between functional monomers and templates in macromolecularly imprinted polymers cannot be as certainly defined as that in MIPs of low-molecular mass template, partly because the hydrogen bond in aqueous media is weaker than that in a nonpolar solvent, and partly because the macromolecules are often flexible and sometimes have undefined structure (distribution of molecular mass). (iii) The removal of the template from the imprinted matrix after polymerization is more difficult in macromolecularly imprinted polymers than in MIPs of low-molecular mass template. Additionally, the following recognition process suffers from the slow mass transport rate of macromolecules. In this article, we provide a simple and versatile solution for macromolecularly imprinted polymers.

The strategic solution for macromolecularly imprinted polymers is surface imprinting conducted in an MIP thin film several tens of nanometers thick, whereas MIP of low-molecular mass template is bulk imprinted in many cases. Some examples have been proposed: (i) surface-initiated atom transfer radical polymerization, in which a radical initiator is first immobilized onto the support/matrix and subsequently template polymerization occurs [3-6]; (ii) the polymer is synthesized first and the MIP process (e.g., precipitation) is subsequently conducted [7-9]; (iii) the template

molecule is adsorbed onto the support/matrix first and the MIP process is subsequently conducted [10]; and (iv) other processes involving material [11,12], supermolecule [13], or hydrogel-based MIP [14]. However, those strategies still are complicated and time-consuming. We envisage the development of macromolecularly imprinted polymers emphasizing simplicity and versatility. Thus, we pursued plasma-induced graft polymerization (PIP) [15-17], in which the plasma pre-treatment is firstly conducted and post-polymerization is secondly completed with residual active species beyond the plasma source. The PIP offers a homogeneously thin coating and can avoid heterogeneous distribution of the binding site, poor site accessibility, and slow mass transport unlike the conventional radical polymerization. Previously, the PIP was applied to the modification of soft materials such as textile, rubber, and plastics because the active species induced by plasma are retained in those systems [15-17]. Only one report of PIP-MIP grafting to polypropylene is chromatography/mass spectroscopy of the low-molecular-weight template pyrethroid [18]. This example of PIP-MIP of low-molecular mass template is an analysis not a sensor. We are applying PIP-macromolecularly imprinted polymers to a biosensor for the first time.

The second issue comprises label-free sensing platforms for integration with MIP, which can pick up direct information on binding events on MIP surfaces. Surface plasmon resonance (SPR) [3,5,9,10] and quartz crystal microbalance (QCM) [7,8,11,14] are the most popular label-free techniques employed in MIP. The mandatory requirement for those label-free techniques is that MIP must be formed onto a flat gold (Au) surface as a homogeneous thin film. We expect that the PIP is the best surface imprinting candidate for macromolecularly imprinted polymers biosensors. Although there are many reports of label-free macromolecularly imprinted polymers biosensors [3,5,7-10,11,14], their binding kinetics have not been evaluated. We present not only the macromolecularly imprinted polymers biosensor (static values) but also binding kinetics (dynamic values) for the first time.

The templates for macromolecularly imprinted polymers are often proteins [3-14], although there are a few reports of polysaccharide MIPs [19-22]. Here, we choose heparin as a model template

for macromolecularly imprinted polymers. Heparin, a highly sulfated polysaccharide, is the most widely used injectable anticoagulant. It is metabolized rapidly by the human body during extracorporeal therapies and surgeries. Although the blood levels of heparin should be monitored continuously during the procedure to ensure the safety of the patient, no reagentless and label-free measuring methods are available for heparin. In our previous study [19,20], electrochemical sensing was performed using heparin-MIP grafted on an indium-tin oxide (ITO) electrode by photo-initiated free radical polymerization. However, this technique for MIP biosensor can be applied only to a transparent ITO electrode and the electrochemical biosensor is neither reagentless nor label-free (using redox marker) because heparin is an electrochemically inactive material. In this study, we demonstrate the characterization and the sensing performance of heparin-PIP-macromolecularly imprinted polymers thin film grafting on an Au electrode for a label-free biosensor for the first time.

2. Experimental

2.1. Materials

Heparin (unfractionated; 130 units per mg; average molecular mass 15,000; from porcine intestinal mucosa), (2-(methacryloxy)-ethyl)trimethylammonium chloride acrylamide (METMAC), acrylamide, N,N-methylenebisacrylamide (MBAA), chondroitin sulfate C (CS) from shark cartilage, and human serum albumin (HSA) were purchased from Wako Pure Chemical Industry Co. Ltd. (Osaka, Japan). Hexamethyldisiloxane (HMDS) was purchased from Aldrich (Milwaukee, WI, USA).

2.2. PIP-MIP synthesis

Figure 1 shows a procedure of PIP-MIP for a label-free biosensor. Condition details are described in the experimental section. First, a plasma-polymerized thin film (PPF) is deposited onto the Au surface. The PPF strongly adheres on the Au surfaces [23]. The PPF deposition on Au surfaces is more effective and continuous than the self-assembly monolayer often used for Au modification in MIP processes [3,5,6,10]. The active species for initiation of post-polymerization remain in the PPF. Plasma treatments were prepared using a plasma deposition system (Model BP-1, Samco International Laboratories, Inc., Kyoto, Japan) incorporating a vacuum pump (Edwards High Vacuum International, West Sussex, UK). An RF generator (Model RFG-300, Samco) was adopted. The working frequency of the power supply was 13.56 MHz. HMDS was introduced from a reservoir. Argon and oxygen were introduced from a gas bombe. A needle

valve was kept fixed during plasma deposition to maintain a stable flow of monomer. The plasma parameters are power: 50-80 W, pressure: 20-30 Pa, flow rate: 1.5 mL min^{-1}, treatment time: 60 s. Subsequently, the PPF/Au electrode is immersed into the solution containing the template, functional monomer, and crosslinker. During aging, double bonds of functional monomer and crosslinker attacked by residually active species in PPF cause a radical chain reaction. Heparin (10 mg), METMAC (28.1 mg; 0.135 mmol), acrylamide (31.3 mg; 0.44 mmol), and MBAA (31.3 mg; 0.20 mmol) were dissolved in 1.5 mL of distilled water, which is the MIP solution. After plasma treatment, the gold electrode is immersed in the MIP solution for 24 h. Consequently, a PIP-MIP thin film network is formed and grafted onto the PPF/Au electrode. Finally, the template on PIP-MIP/PPF/Au is washed out by eluent (0.15 M NaCl). Non-imprinted polymer (NIP) is the same procedure without a template. In addition, a no-plasma-induced MIP was prepared as a control using the same procedure without plasma pre-treatment. One advantage of the PIP-MIP procedure is that it is simpler than any other MIP process.

2.3. Measurements

Ellipsometry was performed with a standard imaging ellipsometer (EP3-SW, λ=532 nm, Nanofilm Technology, Goettingen, Germany). The thicknesses of the thin films were measured by the ellipsometry. Atomic force microscopy (AFM) was conducted in tap ping mode in the ambient atmosphere using a commercial AFM system (NanoScope V Dimension Icon, Bruker AXS GmbH, Karlstruhe, Germany). The scanning tip was silicon cantilever (Nanosensors Inc., AC mode super sharp chip). A scanning rate of 0.3 Hz was employed. AFM system software was used to analyze the image data and calculate defined features, such as the root mean square roughness values (R_{rms}). The QCM instrument used was Q-Sense Explorer (Meiwafosis Co. Ltd., Tokyo, Japan) with 10 mL cells equipped with an AT-cut 5 MHz QCM plate (8 mm diameter quartz plate and an area of 4.9 mm^2 of gold electrode) at the bottom of the cell along with a stirring bar with a temperature control system. Frequency shifts at the third overtones (15 MHz) were employed. The solutions were flowed with a peristatic pump and flow rate was 0.1 mL min^{-1}.

3. Results and Discussion

3.1. Characterization of PIP-MIP thin film

In order to demonstrate the evidence of PIP, Figure 2 shows the thicknesses of PIP-MIP thin films initiated by various precursors of plasma. As a control experiment, it is confirmed that a thin film is not

formed in the no-plasma-induced MIP procedure. Since argon and oxygen plasmas are non-polymerized gases, those do not produce film. The post-polymerization does not occur by argon and oxygen (non-polymerized) plasma pre-treatment but occurs by HMDS (polymerized) plasma pre-treatment. We experimentally demonstrated this fact for the first time. In contrast, the PIP on porous/soft materials such as cellulose [15], cotton [16], polyethylene [17], polypropylene [18], and silicon rubber [18] occurs even if non-polymerized monomer gases (oxygen, argon) are used. The PIP with oxygen and argon plasma initiation does not occur on the surfaces of hard/metal materials. A possible explanation is the following: the plasma can penetrate to a depth of several tens of nanometers, and as a result, the active species for the post-polymerization process are introduced on the surfaces of soft/organic materials; in contrast, the active species for the post-polymerization process cannot be introduced on the surfaces of hard/metal materials; instead, the HMDS PPF deposited on the Au surfaces enables the retention of active species for post-polymerization, in a word, the HMDS PPF plays a role as a scaffold. Since it is known that the free radical remains in the PPF by electron spin resonance measurement [24], the presented mechanism is physicochemically feasible. There are a few documentations of the PIP concept that free radicals are generated during film growth for the initiation of subsequent grafting reaction [25]. Here, the apparent application of PIP involving such concept is presented for the first time.

The optimization of PIP was also conducted as shown in Fig. S1 (Supplementary Material). The parameters are plasma power, plasma treatment time, and post-polymerization time. The results tend to be similar to those of the previous PIP grafting [17,25]. The thickness of PIP is dominated by the amount of retention of active species such as free radicals and peroxides. In order to obtain sufficient MIP thin film, increment of residually active species is required; as a consequence, the pre-PPF scaffold becomes thicker. However, the thicker pre-PPF reduces the sensitivity in PIP-MIP sensors. The optimized thicknesses of PPF (pre-coating scaffold) and PIP-MIP thin film (post-polymerization) were 16 nm and 20 nm, which are ideal values of thickness for surface imprinting as reported by some researchers [3,5,20].

In order to verify PIP-MIP, Figure 3 shows AFM images of PIP-MIP, PIP-NIP, and no-plasma-induced MIP for comparison before and after the removal process of the template (0.15 M NaCl washing). The surface roughnesses (R_{rms}) of PIP-MIP before and after template removal process are different from each other (Fig. 3A and A'), whereas the PIP-NIP (Fig. 3B and B') and no-plasma-induced MIP (Fig. 3C and C') counterparts are almost unchanged. A dimple is observed only on the PIP-MIP surface (Fig. 3A'), whereas it

is not observed on the PIP-NIP (Fig. 3B') and no-plasma-induced MIP (Fig. 3C') counterparts. The diameter and depth of the dimple are ca. 30 nm and 5 nm, which are probably correlated to cavities of the template. Surface morphologies of PIP-MIP and PIP-NIP (Fig. 3A, 3A', 3B, and 3B') are relatively homogeneous, suggesting that the post-polymerization has adequately occurred and the grafting MIP thin film has formed. In contrast, surface morphology of no-plasma-induced MIP (Fig. 3C and C') is rough and inhomogeneous, suggesting that the PIP has not occurred and unreacted materials due to the MIP solution remained. The result indicates that the PIP-MIP is "surface imprinting" and the template removal is successfully achieved.

In order to cross-check the evidence of PIP-MIP, Figure S2 (Supplementary Material) shows XPS measurement of PIP-MIP before and after the removal process of the template. A nitrogen 1s peak originating from a functional monomer (amine group of METMAC) is observed for PIP-MIP with HMDS plasma pre-deposition and is observed for neither no-plasma-induced MIP nor PIP-MIP with argon plasma pre-treatment. A sulfur 2p peak originating from the template (sulfonic acid groups of heparin) has disappeared from the PIP-MIP sample after template removal, indicating that the template is easily washed out from PIP-MIP and not permanently bound. XPS measurement also shows that surface PIP-macromolecularly imprinted polymer is reasonably attained.

3.2. Characterization and sensing performance of PIP-MIP thin film on Au electrode

The characterization and sensing performance of heparin-PIP-macromolecularly imprinted polymers thin film on an Au electrode are demonstrated. The label-free QCM biosensor was used in this study to quantify heparin-PIP-MIP thin film in terms of binding kinetics, detectable range, response time, and selectivity as shown in Fig. 4. The binding compounds from the flowing medium onto the heparin-PIP-MIP/PPF/Au on a quartz surface can be observed with high reproducibility in real time following the frequency shifts. Firstly, the buffer is flowed. After the baseline stabilizes, the binding analyte (heparin, CS, or HSA) is flowed. When the binding event occurs and mass increases, the resonant frequency decreases. After equilibrating the resonance frequency under buffer flowing, binding leads to a significant decrease in frequency to a minimum that represents association with MIP (see k_a in Eqs 1-2). Replacement of the medium by pure buffer solution shows the dissociation of bound compounds from MIP, manifested in a certain frequency increase (see k_d in Eqs 1-2). The

differences between the initial and final frequencies (ΔFs in Fig. 4A-C) represent the binding amount of analyte.

In heparin-PIP-MIP (Fig. 4A-C), the binding amount of heparin ($\Delta F_{heparin}$ in Fig. 4A) is much larger than heparin analog CS (ΔF_{CS} in Fig. 4B) and protein HSA (ΔF_{HSA} in Fig. 4C). The $\Delta F_{heparin}$ are correlated to heparin concentrations whereas the ΔF_{CS} are not correlated to CS concentrations (Fig. 4B). The ΔF_{HSA} is near zero (Fig. 4C), indicating that HSA molecules are generally not retained at the heparin-PIP-MIP surface after reaction. The heparin selective factors toward CS ($\Delta F_{heparin}/\Delta F_{CS}$) at concentrations 0.01 and 0.1 wt% are 2.8 and 5.3, respectively (discussed in the following). The results of three analyte binding tests for heparin-PIP-MIP suggest that heparin-PIP-MIP specifically interacts with heparin.

In heparin-PIP-MIP for 0.1 wt% heparin concentration (Fig. 4A), the sensor signal reaches saturation due to maximum number of binding sites (F_{max}, see Eq 2) on the PIP-MIP surface. Calibration of the 15-MHz QCM (3 overtones of basic oscillation) was performed such that a frequency decrease of 1 Hz corresponded to a mass increase of 5.9 ng cm^{-2} on the QCM electrode from the Sauerbrey equation [26]. The F_{max}=70 Hz estimated in our system corresponds to 410 ng cm^{-2}, which is similar to that of a monolayer of biomacromolecule adsorbed onto a flat surface by QCM [26]. Therefore, we estimate that 27 pmol cm^{-2} of heparin assesses.

In heparin-PIP-MIP for 0.01 and 0.001 wt% heparin concentration (Fig. 4A), the sensor signals do not reach saturation because there is the vacant cavity at the smaller concentration of analyte heparin. This is further evidence of surface imprinting. In heparin-PIP-MIP for 0.001 wt% CS concentration (Fig. 4B), non-Sauerbrey behavior, i.e., increasing frequency, has already been seen for other flat layers where the analyte is only weakly bound on the surface as a non-specific binding and hence retains some mobility [7].

In PIP-NIP (Fig. 4D-F), the binding amounts of all analytes (ΔF) are almost similar when the concentrations are same. This implies that the PIP-NIP does not have a specific binding site and any analytes non-specifically adsorb on the PIP-NIP surface. The amount of heparin adsorption to PIP-NIP is smaller than that to heparin-PIP-MIP and the amounts of CS and HSA adsorption to PIP-NIP are larger than those to heparin-PIP-MIP. This suggests that the heparin-PIP-MIP has heparin-specific binding sites, which also prevent non-specific CS and HSA adsorption.

Figure 5 shows a ΔF vs. concentration plot of the heparin-PIP-MIP and PIP-NIP QCM biosensors. The detectable ranges of heparin in the absence and presence of interferant CS (0.1 wt%) in heparin-PIP-MIP are 0.0005-0.1 wt% and 0.001-0.1 wt%, respectively. Those cover the clinical requirement level. Furthermore, our method is superior in the term of reagentless and label-free as compared to the previous methods of electrochemical sensing with harmful marker [19,20]. In PIP-NIP, there are no differences of binding behavior (relationship between ΔF and concentrations) between heparin and CS, which suggests non-specific adsorption again.

We investigated reusability with the test shown in Fig. S3 (Supplementary Material). The increasing mass on the heparin-PIP-MIP sensing surface due to heparin binding results in a lowering of the resonant frequency, and the flow of 0.15 M NaCl, which removes the template, results in a still lower frequency due to relatively larger viscosity of the 0.15 M NaCl solution. After changing the buffer solution, the frequency recovers the initial level. The following (second) binding event traced the first step, indicating that this is available for a repeatable assay.

The paramount benefit of the QCM biosensor system is that it allows not only sensing but also real-time monitoring of label-free biomolecule-specific interactions, which enables the determination of kinetic parameters such as association (k_a) and dissociation (k_d) coefficients. In order to take this factor into account, the reactions can be represented as [27]:

$$\text{heparin(free)} \underset{k_m}{\overset{k_m}{\rightleftharpoons}} \text{heparin(surface)} + \text{heparin-MIP} \underset{k_d}{\overset{k_a}{\rightleftharpoons}} \text{heparin/heparin-MIP} \qquad (1)$$

where k_a and k_d are the rate constants for interaction between heparin and heparin-PIP-MIP and k_m is the rate constant for mass transport between free (solution) and sensing surface. Because of the surface imprinting, our system is thought to be reaction-controlled (i.e., $k_m > k_a, k_d$) and the rate of surface reaction is given by [28]:

$$\frac{dF}{dt} = k_a C(F_{max} - F) - k_d F \qquad (2)$$

where C is analyte concentration, F is frequency shift of QCM, and F_{max} denotes the surface binding capacity. K_D ($=k_d/k_a$) can be also determined by traditional immunoassay because of the statistic value. Using Eqs 1-2 and numerical data in Fig. 4A, we estimated $k_{a\_heparin}$=350±100 $M^{-1}s^{-1}$, $k_{d\_heparin}$=(5.0±2.0) × 10^{-4} s^{-1}, and $K_{D\_heparin}$=1.3±0.6 μM. The $K_{D\_heparin}$ of heparin/heparin-PIP-MIP is larger than that of

heparin/antithrombin (0.01-0.5 μM) [29]. However, it is smaller than that of antigen/immunoglobulin G (100 μM) and heparin/P-selectin (1.21-5.86 μM) [28]. EL-Sharif et al. reported K_D between hydrogel-based MIP and proteins such as hemoglobin (25 μM), myoglobin (44 μM), and catalase (17 μM) by Scatchard plot [30]. Therefore, the PIP-MIP as a synthetic antibody can be applied to analytical chemistry. Kinetics estimation with a label-free sensing system on biospecific interaction such as antigen-antibody, hormone-receptor, and oligonucleotide association has been frequently reported [27]; however, it has almost never been done on macromolecularly imprinted polymers. This suggests that the PIP provides well-controlled processes facilitating homogeneously macromolecularly imprinted polymers thin film grafting as a sensing element. This shows that the artificial PIP-MIP embedded in the QCM biosensor system can use like antibodies and receptors as natural recognition elements.

Using numerical data in Fig. 4B, we also estimated k_{a_CS}=300±100 $M^{-1}s^{-1}$, k_{d_CS}=(1.2±0.2) × 10^{-3} s^{-1}, and K_{D_CS}=4.0±0.6 μM between CS and heparin-PIP-MIP. The selective factor of heparin toward CS ($K_{D\_heparin}/K_{D\_CS}$) in heparin-PIP-MIP is 4.0, which is not different from the value estimated by the adsorption amount at 0.01-0.1 wt% in Fig. 5 (previously discussed). The origin of heparin selectivity is more attributed to k_d than to k_a from the viewpoint of dynamics; in a word, k_{d_CS} is much larger than $k_{d\_heparin}$ whereas k_{a_CS} is slightly larger than $k_{a\_heparin}$. This suggests that CS bound heparin-PIP-MIP dissociates more rapidly than heparin. The driving force for specific binding is attributed to the electrostatic interaction between the positive charge of trimethylamine groups of the functional monomer and the negative charge of sulfate and carboxylate groups of the template. The trimethylamine groups are positioned in the PIP-MIP backbone. There is a possibility of small molecular size because heparin and CS have the same distribution of molecular mass. The structural difference between heparin and CS is the number of sulfate groups, where heparin and CS have three and one sulfate groups per disaccharide unit. The cross-reaction of CS to heparin-PIP-MIP is attributed to the magnitude of electrostatic interaction. The selectivity is similar to that of other macromolecularly imprinting polymer [3,4,9,12,13]. Therefore, our procedure of PIP-MIP is reasonably attained.

The present strategy can be used not only in label-free (QCM and SPR) biosensors but also in electrochemical biosensors. Figure S4 (Supplementary Material) shows that electrochemical measurement traced the current change due to binding events with a redox marker. The electrochemical system also

showed the selectivity of the PIP-MIP electrode toward a template-like QCM system. The remarkable property is that the redox current of the marker increased when the amount of binding template to the PIP-MIP increased, suggesting that the PIP-MIP has a gate effect like MIP with photo-initiated radical polymerization [19,20]. The gate effect is thought to originate in the change in solute diffusive permeability in the PIP-MIP due to specific binding of the template.

4. Conclusion

We demonstrated a novel fabrication strategy for a heparin-specific MIP on Au surface for a label-free biosensor. An Au electrode grafted with PIP-MIP thin film is suitable for a macromolecularly imprinted polymers biosensor in terms of surface imprinting. The PIP-MIP thin film on Au surface is valid for the polymerized monomer because the PPF by this monomer plays a role as a scaffold for residually active species (radicals) enabling post-polymerization of the solution containing template, functional monomer, and crosslinker. Ellipsometry, AFM, XPS, and QCM experiments show that the PIP-MIP is a suitable strategy for a macromolecularly imprinted polymers biosensor in term of “surface imprinting” where it provides 20 nm thick PIP-MIP layer with a simple procedure. Consequently, the template is easily removed after the PIP-MIP process and the template rapidly accesses the binding cavity of PIP-MIP without a diffusional barrier. The QCM measurement showed that the heparin-PIP-MIP specifically recognized heparin rather than the heparin analog CS where the selective factor was 4.0. The PIP-NIP did not discriminate heparin from CS. The binding kinetics between template and PIP-macromolecularly imprinted polymers is estimated for the first time. Our method can be applied to not only QCM but also surface plasmon resonance and electrochemical sensing. The PIP-macromolecularly imprinted polymers can be easily expanded to other macromolecular templates and can be used in analytical chemistry as a synthetic antibody.

Appendix A. Supplementary material

Supplementary data associated with this article can be found in the online version at http://dx.doi.org/j.jpba.xxx.

References

[1] S. Boulanouar, S. Mezzache, A. Combès, V. Pichon, Molecularly imprinted polymers for the determination of organophosphorus pesticides in complex samples, Talanta 176 (2018) 465-478.

[2] M.J. Whitcombe, I. Chianella, L. Larcombe, S.A. Piletsky, J. Noble, R. Porter, A. Horgan, The rational development of molecularly imprinted polymer-based sensors for protein detection. Chem. Soc. Rev. 40 (2011) 1547-1571.

[3] S. Sasaki, T. Ooya, Y. Kitayama, T. Takeuchi, Molecularly imprinted protein recognition thin films constructed by controlled/living radical polymerization. J. Biosci. Bioeng. 119 (2015) 200-205.

[4] D. Yin, M. Ulbricht, Antibody-imprinted membrane adsorber via two-step surface grafting, Biomacromolecules 14 (2013) 4489-4496.

[5] R. Naraprawatphong, G. Kawanaka, M. Hayashi, A. Kawamura, M. Miyata, Development of protein-recognition SPR devices by combination of SI-ATRP with biomolecular imprinting using protein ligands, Mol. Impr. 4 (2016) 21-30.

[6] H. Zhang, Recent advances in macromolecularly imprinted polymers by controlled radical polymerization techniques, Mol. Impr. 3 (2015) 35-46.

[7] S. Chunta, R. Suedee, P.A. Lieberzeit, Low-density lipoprotein sensor based on molecularly imprinted polymer, Anal. Chem. 88 (2016) 1419-1425.

[8] M. Lee, J.L. Thomas, H. Tseng, W. Lin, B. Liu, H. Lin, Sensing of digestive proteins in saliva with a molecularly imprinted poly(ethylene-co-vinyl alcohol) thin film coated quartz crystal Microbalance Sensor, ACS Appl. Mater. Interfaces 3 (2011) 3064-3071.

[9] M. Tatemichi, M. Sakamoto, M. Mizuhata, S. Deki, T. Takeuchi, Protein-templated organic/inorganic hybrid materials prepared by liquid-phase deposition, J. Am. Chem. Soc. 129 (2007) 10906-10910.

[10] J.R.L. Guerreiro, V.E. Bochenkov, K. Runager, H. Aslan, M. Dong, J.J. Enghild, V.D. Freitas, M.G.F. Sales, D.S. Sutherland, Molecular imprinting of complex matrices at localized surface

plasmon resonance biosensors for screening of global interactions of polyphenols and proteins, ACS Sens. 1 (2016) 258-264.

[11] J. Xu, S. Ambrosini, E. Tamahkar, C. Rossi, K. Haupt, B.T.S. Bui, Toward a universal method for preparing molecularly imprinted polymer nanoparticles with antibody-like affinity for proteins. Biomacromolecules 17 (2016) 345-353.

[12] J. Guo, Y. Wang, Y. Liu, C. Zhang, Y. Zhou, Magnetic-graphene based molecularly imprinted polymer nano composite for the recognition of bovine hemoglobin, Talanta 144 (2015) 411-419.

[13] M. Guo, X. Hu, Z. Fan, J. Liu, X. Wang, Y. Wang, H. Mi, Imprinted polymers with cyclodextrin pseudo-polyrotaxanes as pseudo-supports for protein recognition, Talanta 105 (2013) 409-415.

[14] S.M. Reddy, Q.T. Phan, H. El-Sharif, L. Govada, D. Stevenson, N.E. Chayen, Protein crystallization and biosensor applications of hydrogel-based molecularly imprinted polymers, Biomacromolecules 13 (2012) 3959-3965.

[15] F. Hilt, N.D. Boscher, D. Duday, N. Desbenoit, J. Levalois-Grützmacher, P. Choquet, Atmospheric pressure plasma-Initiated chemical vapor deposition (AP-PiCVD) of poly(diethylallylphosphate) coating: a char-forming protective coating for cellulosic textile, ACS Appl. Mater. Interfaces 6 (2014) 18418-18422.

[16] A. Ramamoorthy, H.M. Helmy, R. Rajbhandari, P. Hauser, A. El-Shafei, Plasma induced graft polymerization of cationic and fluorocarbon monomers into cotton: enhanced dyeability and photostability, Ind. Eng. Chem. Res. 55 (2016) 8501-8508.

[17] G.-H. Hsiue, C.-C. Wang, Functionalization of polyethylene surface using plasma-induced graft copolymerization of acrylic acid. J. Polym. Sci. A Polym. Chem. 31 (1993) 3327-3337.

[18] R. Zhang, X. Guo, X. Shi, A. Sun, L. Wang, T. Xiao, Z. Tang, D. Pan, D. Li, J. Chen, Highly permselective membrane surface modification by cold plasma-induced grafting polymerization of molecularly imprinted polymer for recognition of pyrethroid insecticides in fish, Anal. Chem. 86 (2014) 11705-11713.

[19] Y. Yoshimi, R. Inaba, T. Ogawa, W. Yoshino, M. Inoue, K. Kuwana, Stabilized sensing of heparin in whole blood using the 'gate effect' of heparin-imprinted polymer grafted onto An electrode, Mol. Impr. 4 (2016) 13-20.

[20] Y. Yoshimi, K. Sato, M. Ohshima, E. Piletska, Application of the 'gate effect' of a molecularly imprinted polymer grafted on An electrode for the real-time sensing of heparin in blood, Analyst 138 (2013) 5121-5128.

[21] L. Li, Y. Liang, Y. Liu, Designing of molecularly imprinted polymer-based potentiometric sensor for the determination of heparin, Anal. Biochem. 434 (2013) 242-246.

[22] F. Li, J. Li, S. Zhang, Molecularly imprinted polymer grafted on polysaccharide microsphere surface by the sol–gel process for protein recognition, Talanta 74 (2008) 1247-1255.

[23] H. Muguruma, Plasma-polymerized films for biochip design. Plasma Process. Polym. 7 (2010) 151-162.

[24] M. Kuzuya, A. Noguchi, M. Ishikawa, A. Koide, K. Sawada, A. Ito, N. Noda, Electron spin resonance study of free-radical formation and its decay of plasma-induced poly(methacrylic acid) and its esters, J. Phys. Chem. 95 (1991) 2398-2403.

[25] F. Khelifa, S. Ershov, Y. Habibi, R. Snyders, P. Dubois, Use of free radical on the surface of plasma polymer for the initiation of a polymerization reaction, ACS Appl. Mater. Interfaces 5 (2013) 11569-11577.

[26] H. Muguruma, Y. Kase, N. Murata, K. Matsumura, Adsorption of glucose oxidase onto plasma-polymerized film characterized by atomic force microscopy, quartz crystal microbalance, and electrochemical measurement, J, Phys. Chem. B 110 (2006) 26033-26039.

[27] D.G. Myszka, Kinetic analysis of macromolecular interactions using surface plasmon resonance biosensors, Current Opinion Biotech. 8 (1997) 50-57.

[28] D. Simonis, J. Fritzsche, S. Alban, G. Bendas, Kinetic analysis of heparin and glucan sulfates binding to P-selectin and its impact on the general understanding of selectin inhibition, Biochemistry 46 (2007) 6156-6164.

[29] V. Arocas, B. Turk, S.C. Bock, S.T. Olson, I. Björk, The region of antithrombin interacting with full-length heparin chains outside the high-affinity pentasaccharide sequence extends to Lys136 but not to Lys139, Biochemistry 39 (2000) 8512-8518.

[30] H.F. EL-Sharif, D.M. Hawkins, D. Stevenson, S.M. Reddy, Determination of protein binding affinities within hydrogel-based molecularly imprinted polymers (hydroMIPs). Phys. Chem. Chem. Phys. 16 (2014) 15483-15489.

Figure captions

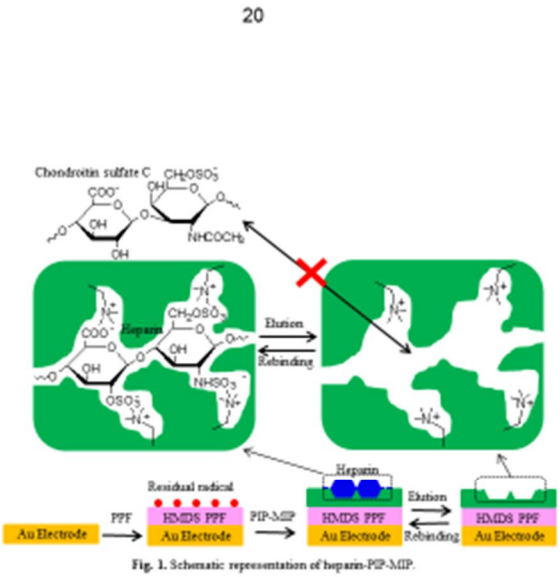

Fig. 1. Schematic representation of heparin-PIP-MIP.

21

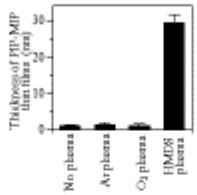

Fig. 2. Thickness of MIP thin films fabricated by PIP with various plasma precursors.

Fig. 2. Thickness of MIP thin films fabricated by PIP with various plasma precursors.

22

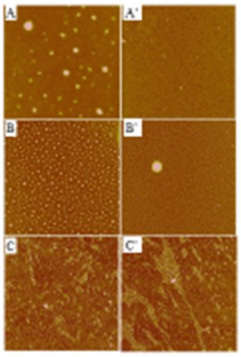

Fig. 3. AFM images of (A,A') PIP-MIP, (B,B') PIP-NIP, and (C,C') no-plasma-initiated MIP before (A-C) and after (A'-C') washing by 0.15 M NaCl. Horizontal scale: 5×5 μm. Vertical scale: 10 nm. Surface roughness (R_{rms}): (A) 0.822 nm, (A') 0.498 nm, (B) 0.702 nm, (B') 0.675 nm, (C) 1.01 nm, (C') 1.03 nm.

Fig. 3. AFM images of (A,A') PIP-MIP, (B,B') PIP-NIP, and (C,C') no-plasma-induced MIP before (A-C) and after (A'-C') washing by 0.15 M NaCl. Horizontal scale: 5×5 μm. Vertical scale: 10 nm. Surface roughness (R_{rms}): (A) 0.822 nm, (A') 0.498 nm, (B) 0.702 nm, (B') 0.675 nm, (C) 1.01 nm, (C') 1.03 nm.

23

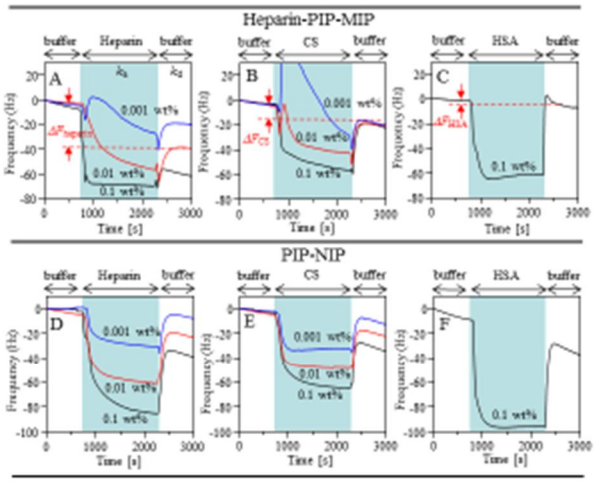

Fig. 4. Frequency vs. time plots of various concentrations of heparin, CS, and HSA as analytes of heparin-PIP-MIP and PIP-NIP QCM biosensors.

Fig. 4. Frequency vs. time plots of various concentrations of heparin, CS, and HSA as analytes of heparin-PIP-MIP and PIP-NIP QCM biosensors.

24

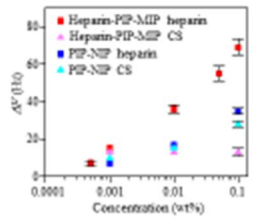

Fig. 5. Frequency vs. concentration plots of heparin and CS as analytes of heparin-PIP-MIP and PIP-NIP QCM biosensors.

Fig. 5. Frequency vs. concentration plots of heparin and CS as analytes of heparin-PIP-MIP and PIP-NIP QCM biosensors.